Supporting information

Bandgap Tuning of Silver Bismuth Iodide via Controllable Bromide Substitution for Improved Photovoltaic Performance

Authors Names: Hua Wu,[1,2] Huimin Zhu,[1] Axel Erbing,[3] Malin B. Johansson,[1] Soham Mukherjee,[4] Gabriel J. Man,[4] Håkan Rensmo,[4] Michael Odelius,[3] Erik M. J. Johansson[1,*]

AUTHOR ADDRESS:

[1] Department of Chemistry—Ångström-Laboratory, Institution of Physical Chemistry, Uppsala University, Uppsala 75120, Sweden

[2] State Key Laboratory on Integrated Optoelectronics and College of Electronic Science and Engineering, Jilin University 130012, Changchun, China

[3] Department of Physics, Stockholm University, AlbaNova University Center, Stockholm 10691, Sweden

[4] Molecular and Condensed Matter Physics, Department of Physics and Astronomy, Uppsala University, Uppsala 75120, Sweden

AUTHOR INFORMATION

Corresponding Author

Erik M. J. Johansson

*Email address: erik.johansson@kemi.uu.se

Experimental section:

Chemicals:

Bismuth iodide (BiI_3, 99.99%), silver iodide (AgI, 99%), bismuth bromide ($BiBr_3$, 98%), Poly [[2,3-bis(3-octyloxyphenyl)-5,8-quinoxalinediyl]-2,5-thiophenediyl] (TQ1), titanium(IV) isopropoxide (TTIP, 97%), dimethyl sulfoxide (DMSO, anhydrous, 99.8%) and chlorobenzene (CB, 99.8%) were obtained from Sigma-Aldrich. All solvents were used without further purification.

Absorber film fabrication:

Here, $BiBr_3$ was used as the source of Br, since AgBr is insoluble in DMSO solvent, even when heating the AgBr solution at a high temperature. The precursor solutions were obtained by dissolving AgI (0.5mmol, 117 mg), BiI_3 and $BiBr_3$ powder in 1ml DMSO solvent. The relative amounts of BiI_3 and $BiBr_3$ were varied to obtain mixed halide materials, while the total Bi concentration, $[Bi^{3+}]$, in the final solution was kept at 1M. The mixed solutions were kept stirred under 100 ^oC until the solution turned transparent. UV-ozone treatment was applied to substrates before spin-coating. Then the treated substrates were transferred to a dry box (filled with nitrogen, 20% relative humidity) for fabrication of absorber films. The clear precursor solution was spin-cast on substrates at 6000 rpm for 30 seconds. Then the films were annealed at 90 ^oC for 5 min and 150 ^oC for 15 min. During the annealing process, the color of the absorber films changed. The samples were characterized when they had cooled down to room temperature.

Device fabrication:

For fabrication of solar cell devices, FTO-coated glass was firstly cleaned by using soap solution, deionized water, acetone and ethanol. To deposit the TiO_2 compact layer, a solution (containing 1 mL of TTIP and 9 mL of ethanol) was sprayed onto FTO glass heating on a hot plate at 500 ^oC for 30 min. For deposition of the TiO_2 mesoporous layer, the paste was prepared by diluting Dyesol paste (30 nm of particle size) with ethanol in a 2/7 weight ratio. After spin-coating the paste at 4000 rpm, the films were heated at 500 ^oC for 30 min. The

absorber films were made following the method mentioned in previous section. The hole transport layer of was deposited by spin-coating TQ1/CB (dissolving TQ1 in CB solvent at concentration of 10 mg·mL^{-1}) solution at 2500 rpm. Finally, gold layer with a thickness of 80 nm was evaporated using a thermal deposition method under vacuum of around 10^{-5} mbar.

Solar cell characterizations:

Power conversion efficiency (PCE): The current-voltage curves of the devices were measured with a Keithley 2400 source meter under 1 sun AM 1.5 G (100 mW·cm^{-2}) illumination, under a scanning speed of 100 mV/s. The sunlight was provided by a solar simulator (Model: 91160), and calibrated using a standard Si solar cell. All solar cells were illuminated from the working electrode (glass substrate) side with an active area of 0.124 cm^2 (circular shaped mask).

Incident photon to current conversion efficiency (IPCE): The IPCE spectra were recorded using a Keithley 2700 multimeter and a monochromator (Spectral Products, CM 110), providing monochromatic light. Before measurement, the system was calibrated via the standard Si solar cell.

Carrier lifetime measurements: For recording carrier lifetimes, a computer-controlled setup consisting of a white LED (ST-210WHF, Seventeam) as light source, and a 16-bit resolution digital acquisition board (BNC-2110, National Instruments) to record voltage were employed. Carrier lifetimes were determined by the photovoltage transient's process by applying a square wave modulation onto the base light illumination. Finally, the lifetime values were obtained by fitting the photovoltage response curves.

Film characterizations:

UV-vis spectra: The reflectance and transmittance spectra were measured via a Lambda 900 double-beam UV/vis/NIR spectrophotometer, equipped with an integrating sphere and a Spectralon reflectance standard. The absorbance A(λ) was calculated following relationship: A(λ)=100-R(λ)-T(λ), where R represents reflectance and T represents transmittance. The calculation of the absorption coefficient was following a previous reported method.[1]

X-ray diffraction (XRD): XRD patterns were measured using a Siemens D5000θ−2θ goniometer with CuKα (λ =1.54051 Å) radiation and 0.4° Soller-slit collimator which with a resolution of 0.3° (2θ) (Bruker AXS, Karlsruhe, Germany).

Scanning electron microscopy (SEM): The surface images of films, cross-section image of device and mapping results were obtained by employing a LEO 1550 FEG instrument and a secondary electron detector operating at 5 kV (10 KV for mapping).

Theoretical section

DFT calculation method: Electronic structure calculations using density functional theory were performed on eight different halide compositions ranging from $AgBi_2I_7$ to $AgBi_2Br_7$. Cell and geometry optimizations were performed on the generated structures using the CP2K package[2] with the Gaussian and plane waves (GPW) method and Godecker-Teter-Hutter (GTH) pseudopotentials[3-4] in the Quickstep (QS) code[5]. The electron density was described by a plane-wave basis set with an energy cutoff of 600 Ry and the Kohn-Sham orbitals were expanded in a local Gaussian TZVP basis set (generated following[6] and distributed with the CP2K program). The calculations were performed using the PBE functional augmented with Van der Waals-interactions[7] at a mesh of 27 k-points equally spaced in the Brillouin zone, generated following the Monkhorst-Pack scheme[8]. In the optimization, both the atomic coordinates and the cell parameter *a* were allowed to vary freely while keeping the cubic symmetry of the simulation cell. From the optimized structure and wavefunction, individual calculations of single k-points along specific lines in the Brillouin zone were computed yielding information about the band structure for the different compositions. Density of states (DOS) and partial density of states (PDOS) calculations were also performed on a 2x2x2 multiple unit cell, i.e. a super cell with the unit cell halide distribution, of the optimized structures for Kohn-Sham orbitals obtained for the Γ point without k-point sampling. Here the energies of the Kohn-Sham orbitals are employed in the interpretation of the photoelectron spectra and the orbital energies of the occupied orbitals are associated with the electron binding energies. An ad-hoc shift of the energy was applied so that zero energy corresponds to middle of the band gap. To directly compare to experiments, the obtained DOS and PDOS were convoluted by a Gaussian function with a full width at half-maximum of 0.4 eV.

The cubic $AgBi_2I_7$ crystal structure is modeled after the cubic $AgBiI_4$ crystal , with different lattice site occupations, as discussed in reference[9].

$AgBiI_4$ has the space group $Fd\bar{3}m$ and a reported lattice parameter of 12.223 Å, described in more detail in reference[10]. The unit cell contains 5 Ag, 9 Bi, and 32 I, which results in two vacancies at cation sites. Hence, as a consequence of the uncertainty in the relative position of the vacancies, the structure of the crystal is not uniquely defined, and different structures needed to be evaluated. A set of approximately 30 structures were constructed, in which the Ag, Bi, and vacancies were initially distributed randomly into the cation lattice sites. However, subsequent cell and geometry optimizations revealed that some structures were more stable energetically than others and resulted in smaller changes to the initial structure. An energetic comparison of different structures of the pure iodine composition revealed that high-energy configurations resulted in the Ag atoms completely leaving their cation sites and form clusters. The phenomenon seems to be strongly dependent on the relative positions of the Ag atoms and the vacancies and this effect of diffusion will be investigated in a future study. Within this study, one low-energy configuration of cations and vacancies, in which the Ag atoms are stable in the crystal lattice during optimization, is used in all calculations at different halide composition. The specific details of this cation configuration are provided in in Table S1 and the systems will be further investigated in ongoing and future work. Note that the anion positions are unambiguous. The compositions containing Br were obtained by randomly substituting I atoms until the desired halide ratio was obtained.

Table S1 Atomic coordinates of the cation configuration, given in terms of the lattice constant, used in the calculations.

Element	x	y	z
Ag	0.00	0.00	0.00
Ag	0.25	0.25	0.00
Ag	0.25	0.50	0.75
Ag	0.25	0.75	0.50
Ag	0.50	0.00	0.50

Bi	0.75	0.75	0.00
Bi	0.75	0.25	0.50
Bi	0.25	0.00	0.25
Bi	0.00	0.25	0.25
Bi	0.50	0.25	0.75
Bi	0.00	0.75	0.75
Bi	0.50	0.50	0.00
Bi	0.50	0.75	0.25
Bi	0.00	0.50	0.50

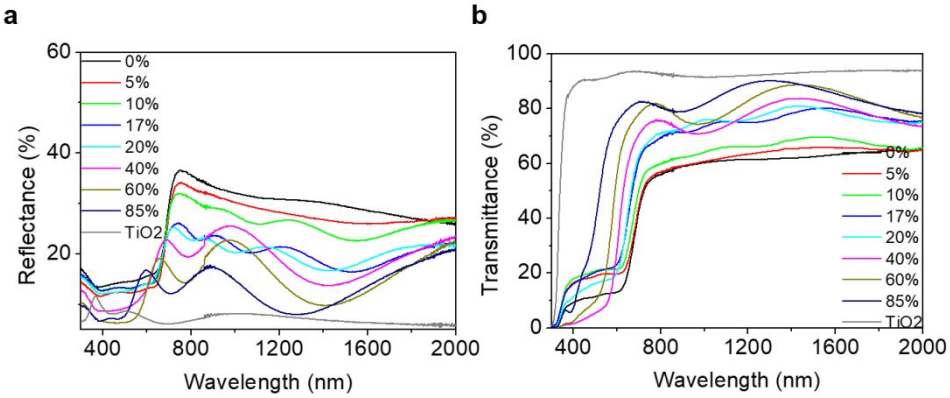

Figure S1 The total reflectance spectra (a) and transmittance spectra (b) of films with different amount Br incorporation (deposited on TiO_2 substrates)

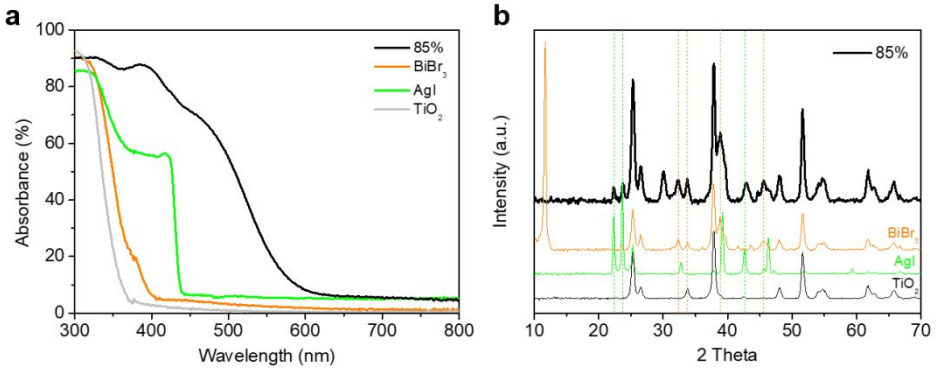

Figure S2 The comparison of absorption (a) and XRD patterns (b) for 85%-Br incorporated film, precursor materials and TiO_2 substrate.

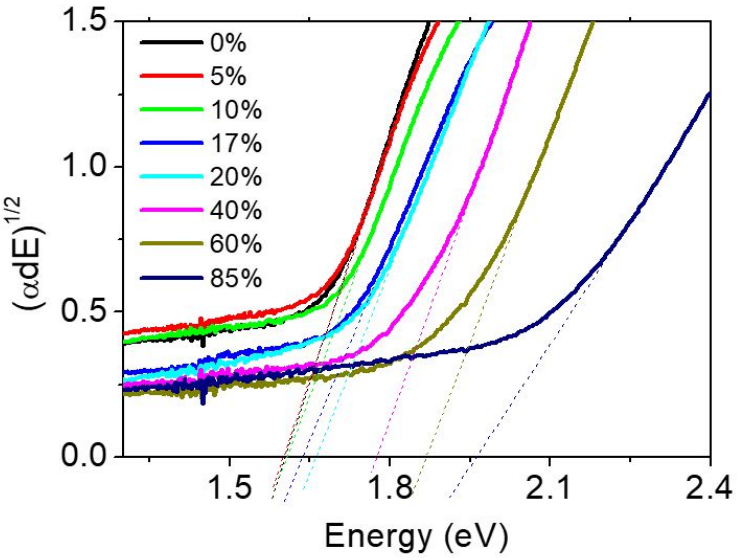

Figure S3 The indirect optical transitions estimated from absorption coefficients of these films.

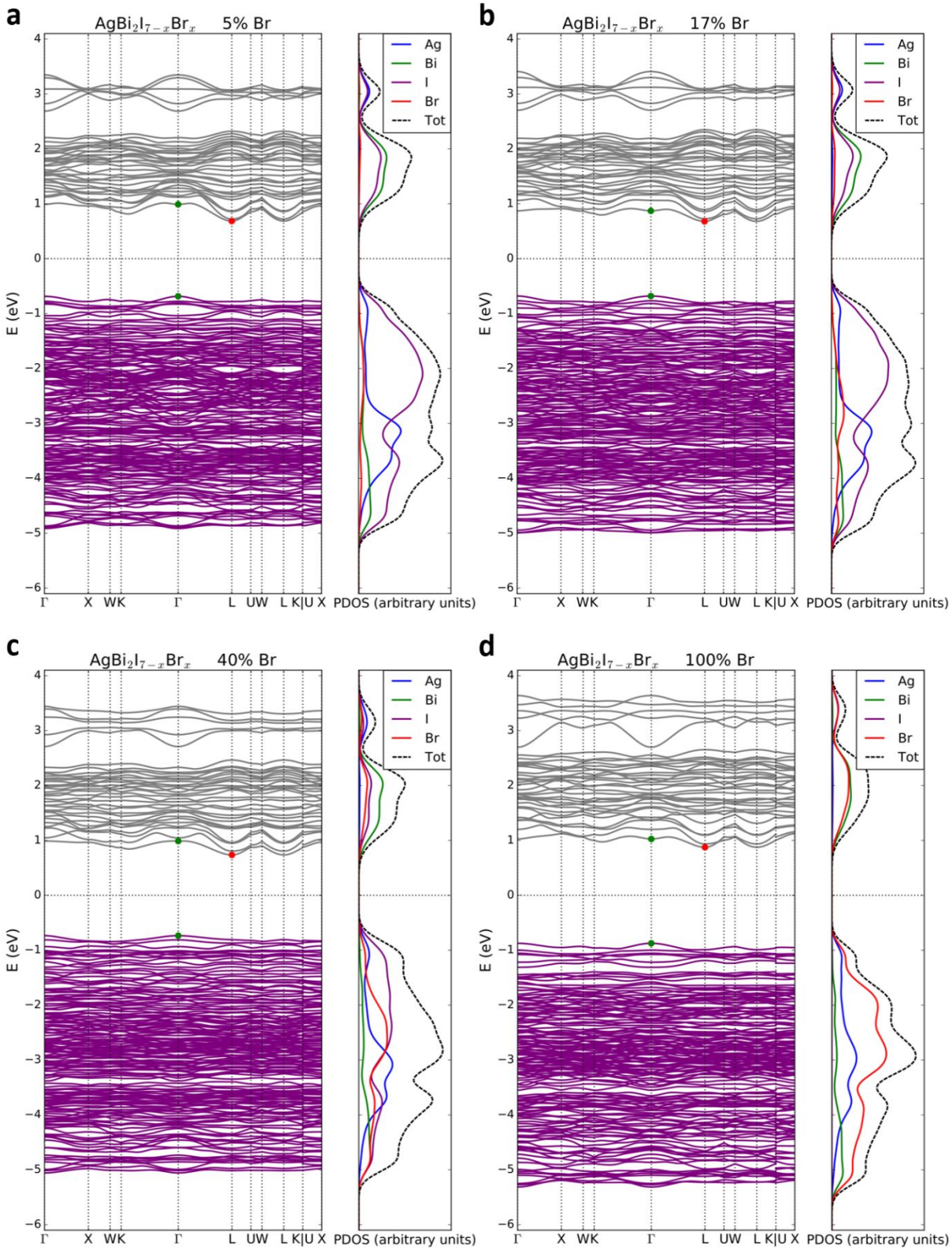

Figure S4 The band structure diagrams and plots of the projected density of states for the following samples: (a) 5%, (b) 17%, (c) 40% and (d) 100% bromide incorporation. E = 0 (the middle of the bad gap) is denoted with a dashed line.

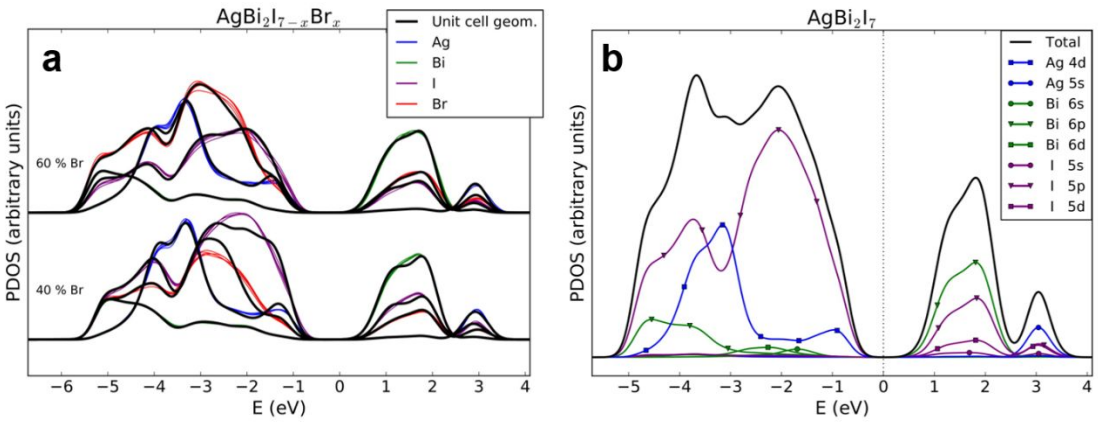

Figure S5 (a) The difference in PDOS between the 2x2x2 multiple unit cell representation using the unit cell geometry and five relaxed super-cell realizations. Notice that smaller local deviations occur but the results are qualitatively the same. The halide compositions closer to full bromine and iodine showed significantly less discrepancy. (b) The PDOS of $AgBi_2I_7$ with more details and with additional states displayed separately.

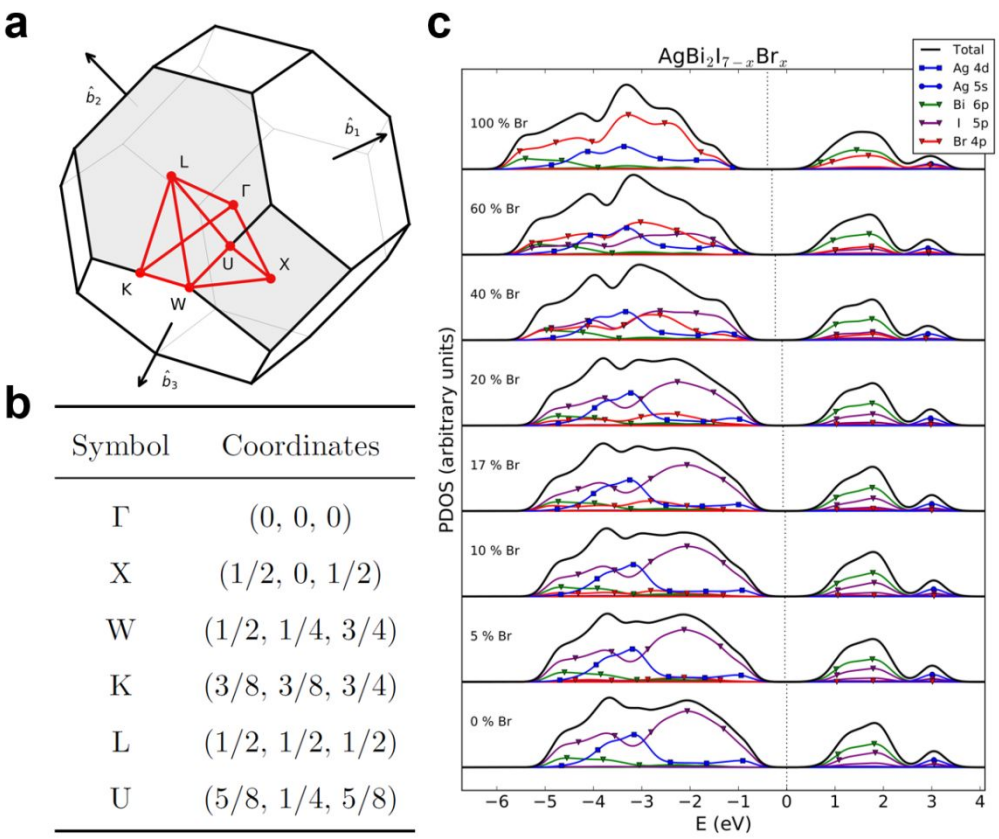

Symbol	Coordinates
Γ	(0, 0, 0)
X	(1/2, 0, 1/2)
W	(1/2, 1/4, 3/4)
K	(3/8, 3/8, 3/4)
L	(1/2, 1/2, 1/2)
U	(5/8, 1/4, 5/8)

Figure S6 (a) the first Brillouin zone of a face centered cubic (fcc) lattice. (b) Points of high symmetry of an fcc lattice. The coordinates are given in terms of the reciprocal basis vectors

$\hat{b}_1 = \frac{2\pi}{a}(-1, 1, 1)$, $\hat{b}_2 = \frac{2\pi}{a}(1, -1, 1)$, and $\hat{b}_3 = \frac{2\pi}{a}(1, 1, -1)$. (c) the summary of PDOS plots for all samples with varying Br amount.

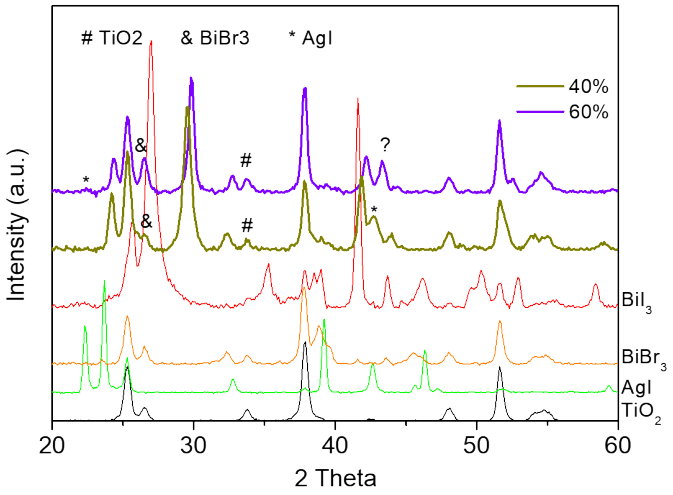

Figure S7 Comparison of XRD patterns for absorber films, precursor films (BiI_3, $BiBr_3$ and AgI) and TiO_2 substrates.

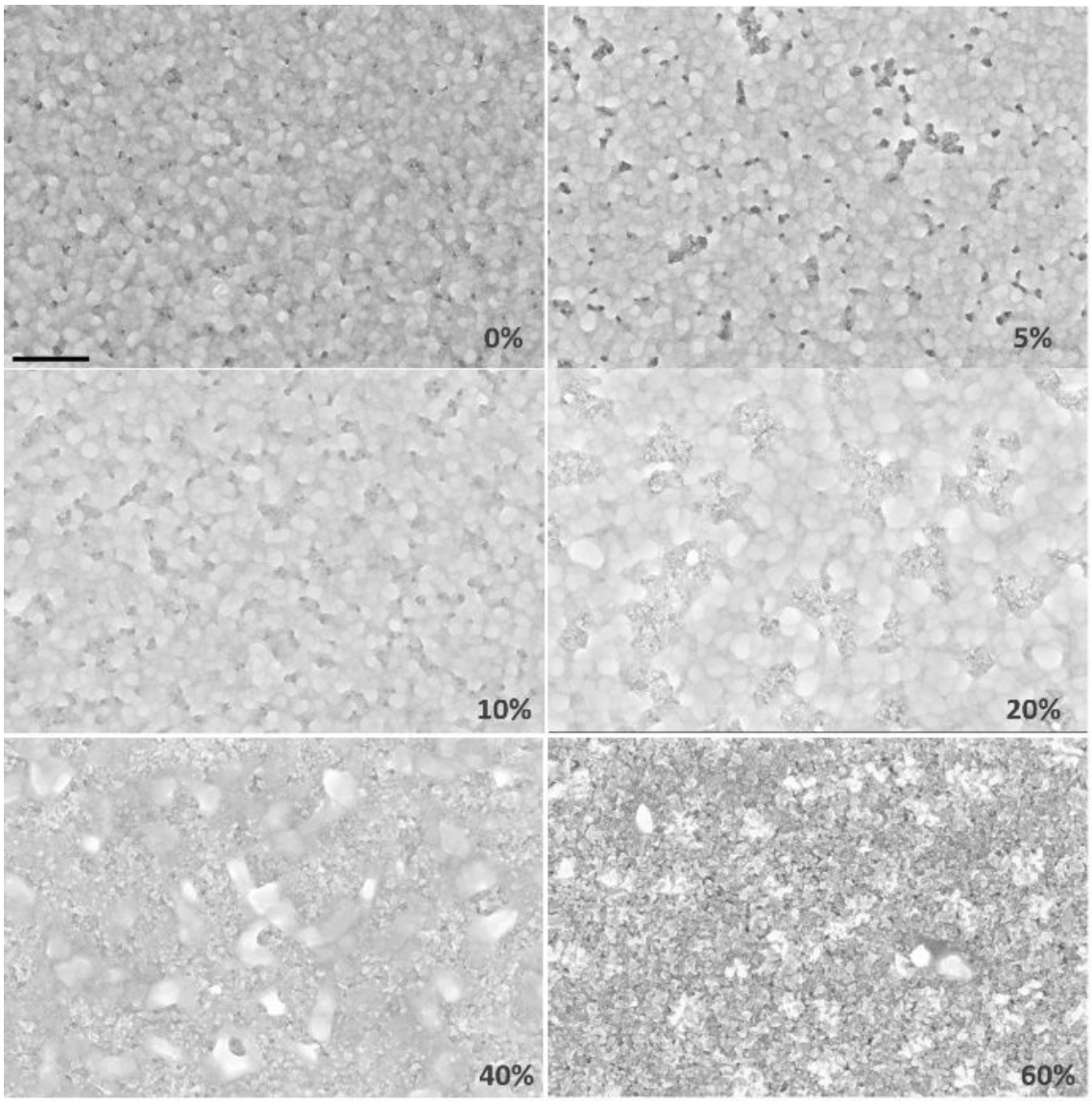

Figure S8 The surface SEM images from films with different amount Br. The scale bar represents 1 μm.

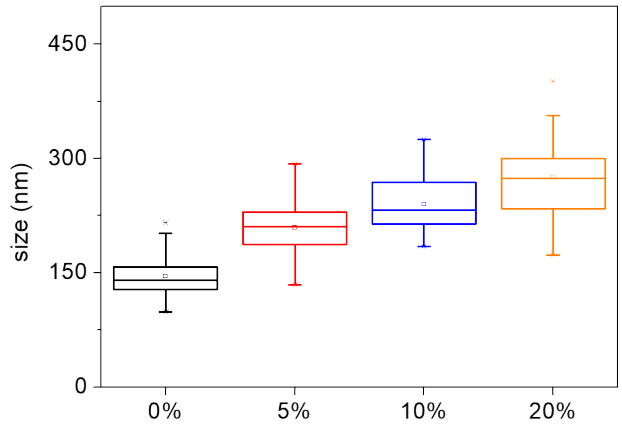

Figure S9 The distribution of grain sizes of films with various degree of Br incorporation from 30 grains for each film.

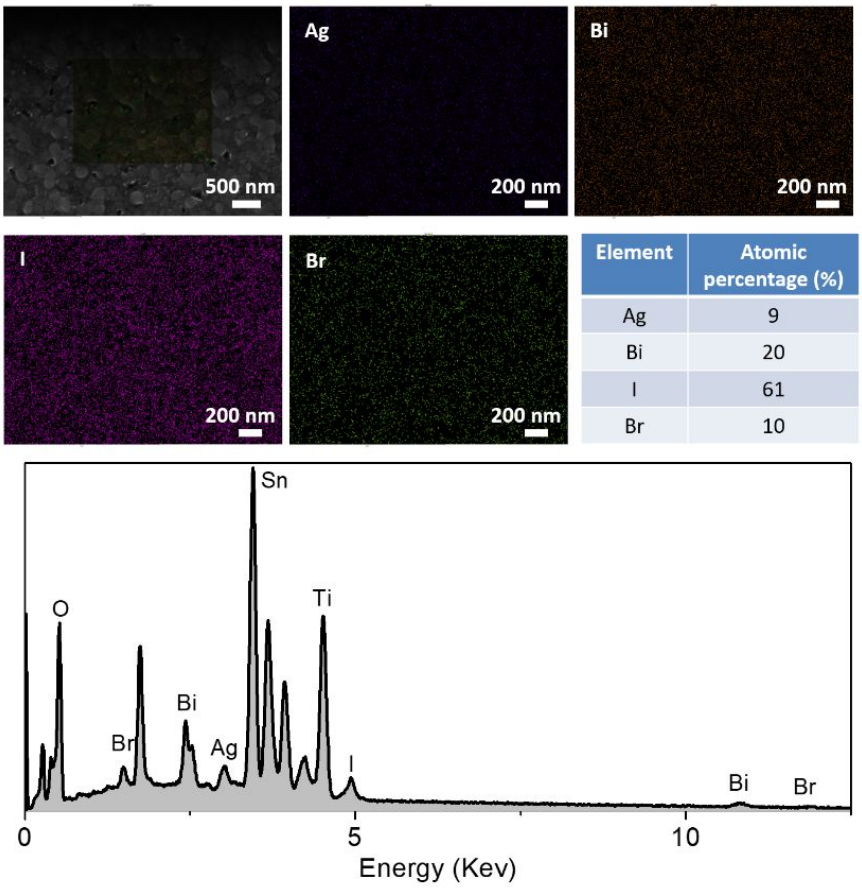

Element	Atomic percentage (%)
Ag	9
Bi	20
I	61
Br	10

Figure S10 EDX measurement of 10%-doped sample, showing the elements' distribution and composition at the sample.

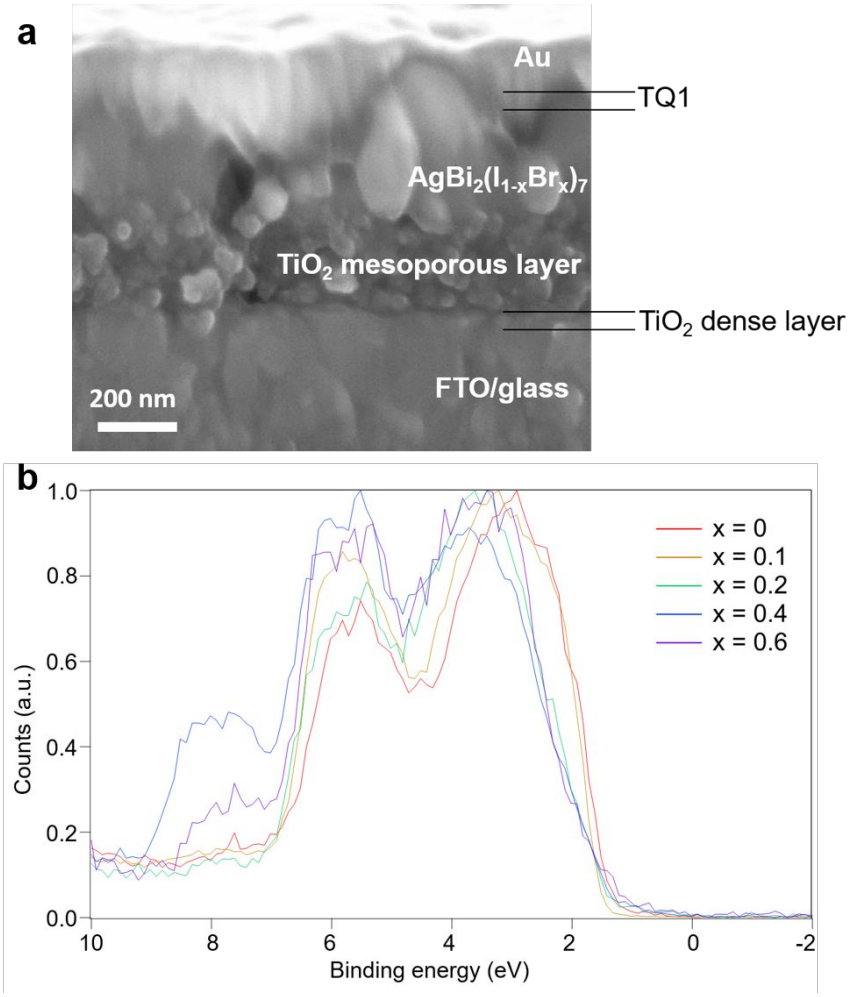

Figure S11 (a) A cross-sectional SEM image from a device fabricated under the conditions of the best-performed cell; (b) XPS valence band spectra for $AgBi_2(I_{1-x}Br_x)_7$ with various Br amount.

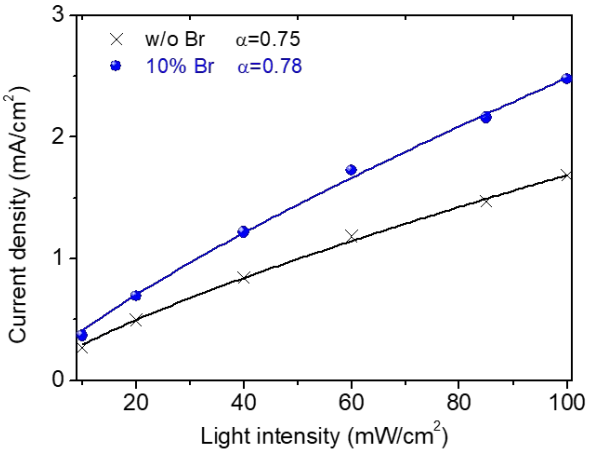

Figure S12 The light intensity-dependent current density for solar cell devices with pure iodide and 10%-bromide doped films.

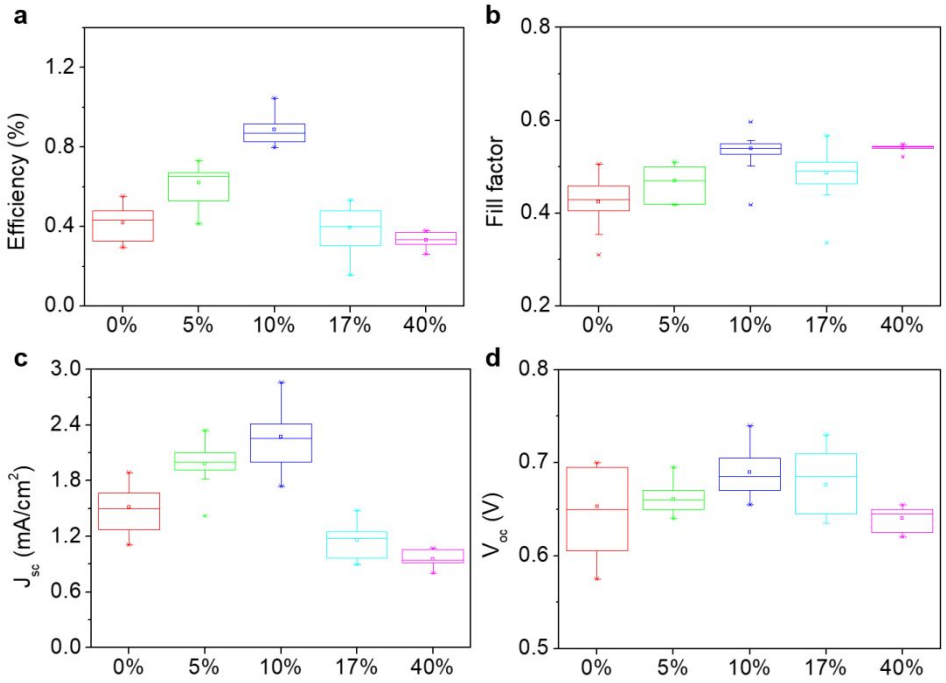

Figure S13 The distribution of parameters from solar cells based on different degree of Br incorporation: (a) efficiency, (b) fill factor, (c) J_{SC}, and (d) V_{OC} for 16 solar cells, respectively.

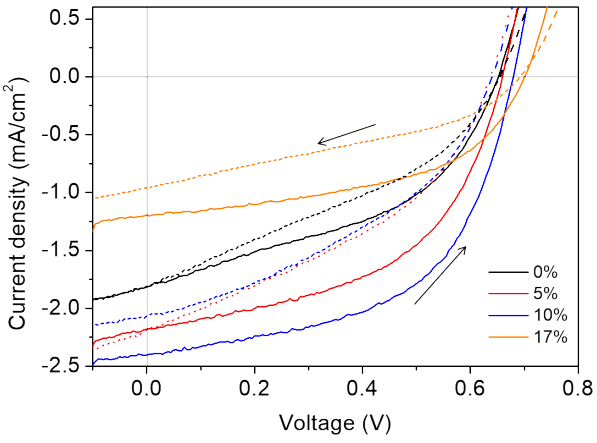

Figure S14 The J-V curves under forward and reverse scan of devices based on different amount Br doping, where solid lines represent forward scan and dash lines represent reverse scan.

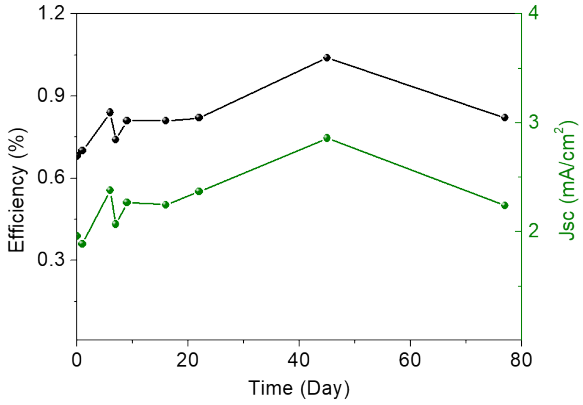

Figure S15 The performance evolution of the device based on 10%-doping, while the device was unencapsulated and stored in air under dark environment.

References:

1. Johansson, M. B.; Zhu, H.; Johansson, E. M. J., Extended Photo-Conversion Spectrum in Low-Toxic Bismuth Halide Perovskite Solar Cells. *J Phys. Chem. L* **2016,** *7* (17), 3467-3471.

2. CP2K Version 6.1 the CP2K developers group. http://www.cp2k.org, 2019-03-15

3. Goedecker, S.; Teter, M.; Hutter, J., Separable dual-space Gaussian pseudopotentials. *Physical Review B* **1996,** *54* (3), 1703.

4. Krack, M., Pseudopotentials for H to Kr optimized for gradient-corrected exchange-correlation functionals. *Theor. Chem. Acc.* **2005,** *114* (1-3), 145-152.

5. VandeVondele, J.; Krack, M.; Mohamed, F.; Parrinello, M.; Chassaing, T.; Hutter, J., Quickstep: Fast and accurate density functional calculations using a mixed Gaussian and plane waves approach. *Comput. Phys. Commun.* **2005,** *167* (2), 103-128.

6. VandeVondele, J.; Hutter, J., Gaussian basis sets for accurate calculations on molecular systems in gas and condensed phases. *J. Chem. Phys.* **2007,** *127* (11), 114105.

7. Perdew, J. P.; Burke, K.; Ernzerhof, M., Generalized gradient approximation made simple. *Phys. Rev. Lett.* **1996,** *77* (18), 3865.

8. Monkhorst, H. J.; Pack, J. D., Special points for Brillouin-zone integrations. *Phys. Rev. B* **1976,** *13* (12), 5188.

9. Xiao, Z.; Meng, W.; Mitzi, D. B.; Yan, Y., Crystal Structure of $AgBi_2I_7$ Thin Films. *J Phys. Chem. L* **2016,** *7* (19), 3903-3907.

10. Oldag, T.; Aussieker, T.; Keller, H.-L.; Preitschaft, C.; Pfitzner, A., Solvothermale Synthese und Bestimmung der Kristallstrukturen von $AgBiI_4$ und Ag_3BiI_6. *Z. Anorg. Allg. Chem.* 2005, 631, 677-682